nature catalysis

Article

https://doi.org/10.1038/s41929-023-00943-2

Reaction environment impacts charge transfer but not chemical reaction steps in hydrogen evolution catalysis

Received: 11 September 2022

Accepted: 8 March 2023

Published online: 26 April 2023

Check for updates

Bryan Y. Tang, Ryan P. Bisbey, Kunal M. Lodaya, Wei Lun Toh & Yogesh Surendranath

Interfacial electrocatalysis involves elementary chemical and charge transfer reaction steps. For the hydrogen evolution reaction (HER), the applied overpotential can be partitioned into a charge transfer overpotential, which drives proton-coupled electron transfer, and a chemical overpotential arising from increasing surface H activity. However, typical experiments report on the aggregate rate–overpotential profile, with no information about the relative contributions from these two components. Herein, we employ a Pd membrane double cell to spatially isolate charge transfer and chemical reaction steps in HER catalysis, deconvoluting their overpotential contribution under different reaction conditions. We analyse how pH and the introduction of poisons and promoters affect each component, and find that for a given H_2 release rate, only the charge transfer overpotential is affected by reaction conditions. These findings suggest that reaction-condition-dependent HER efficiencies are driven predominantly by changes to the charge transfer kinetics rather than the chemical reactivity of surface H.

The interconversion of electrical and chemical energy requires catalysts that can mediate complex multi-electron, multi-proton reactions. When the electrocatalyst itself is the electrode, it facilitates these complex reactions by binding and stabilizing surface intermediates[1,2]. Thus, an overall electrocatalytic mechanism invariably consists of a sequence of elementary reaction steps that can be broadly bifurcated as either charge transfer steps (those involving the transit of ions across the electrical double layer to form surface-bound intermediates) or chemical reaction steps (those involving the reaction of those surface intermediates with each other)[3,4]. The rational design of improved electrocatalysts requires a detailed understanding of the relative contributions from charge transfer and chemical reaction kinetics to the overall reaction efficiency and how each depends on key reaction variables such as electrolyte, pH and potential.

The thermochemistry and kinetics of both the charge transfer and chemical reaction steps are affected by the applied potential. This underappreciated concept can be understood in the context of the hydrogen evolution reaction (HER). In one viable mechanism for the HER (the Volmer–Tafel mechanism), the key surface H intermediate, historically termed overpotential deposited H (H_{OPD}), is first formed through proton-coupled electron transfer (PCET). This is followed by a chemical reaction step wherein two H_{OPD} species recombine to form H_2 (Fig. 1)[5,6]. For this mechanism, changes to the applied potential serve to directly increase the driving force and rate of the charge transfer step. This higher rate of H_{OPD} formation must be balanced by an equally higher rate of H_{OPD} recombination to form H_2 at steady state. Thus, the H_{OPD} surface coverage will increase until the rates of H_{OPD} formation via charge transfer and consumption via recombination are matched[7–9]. This indirect change in the H_{OPD} coverage and corresponding activity (a_H) can be viewed as a chemical overpotential, $\eta_{chemical}$ (Fig. 1), which, in this context, is the change in the chemical potential of surface H (μ_H) relative to its value in equilibrium with 1 atm H_2 ($\mu_{H,0}$, defined as μ_H at the reversible hydrogen electrode (RHE) potential), such that:

Department of Chemistry, Massachusetts Institute of Technology, Cambridge, MA, USA. e-mail: yogi@mit.edu

https://doi.org/10.1038/s41929-023-00943-2

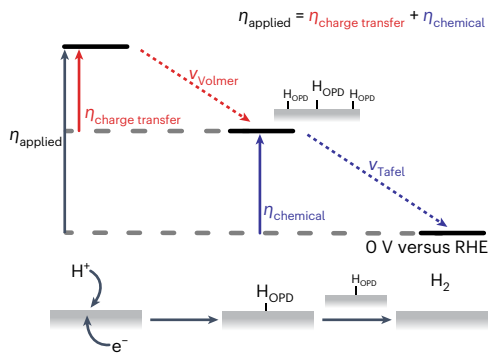

Fig. 1 | Hydrogen electrocatalysis on electrode surfaces is composed of both chemical and charge transfer overpotential components. Free energy schematic for the electrochemical HER, with H_{OPD} as the key surface intermediate for the reaction. Under polarization, the applied overpotential ($\eta_{applied}$) is the aggregate of two overpotential components, the $\eta_{charge\ transfer}$ and the $\eta_{chemical}$. Under steady-state conditions, the rates of H_{OPD} generation and H_{OPD} consumption must be equal to one another (v_{Volmer} and v_{Tafel}, respectively, in a Volmer–Tafel mechanism).

$$\eta_{chemical} = \frac{\mu_H - \mu_{H,0}}{F} = \frac{RT}{F} \ln \frac{a_H}{a_{H,0}} \quad (1)$$

where $a_{H,0}$ is the chemical activity of surface H at the RHE potential in the presence of 1 atm of H_2 (see Supplementary Note 1 for derivation), F is Faraday's constant, R is the gas constant and T is temperature.

Within this framework, the overall overpotential for HER catalysis partitions into a fraction going towards accelerating the rate of the charge transfer step to form H_{OPD}. We define this as the charge transfer overpotential, $\eta_{charge\ transfer}$ (Fig. 1). The remainder goes towards accelerating the rate of the chemical reaction step for forming H_2 ($\eta_{chemical}$)[7]. Although the foregoing logic emphasizes, qualitatively, that both $\eta_{charge\ transfer}$ and $\eta_{chemical}$ vary with the applied potential, the quantitative partitioning between the two is unknown. This is because a typical polarization experiment only reports on the aggregate current–overpotential profile, and thus, contains no information about the individual overpotential contributions that affect the charge transfer and chemical steps.

It is now widely appreciated that the overall kinetics of HER are strongly dependent on reaction conditions: on noble metals, HER kinetics are attenuated by two orders of magnitude in base compared with acid[10–15]; the presence of alkali cations and buffering anions in the electrolyte can promote HER kinetics[16–19]; and surface-bound species are known to both promote[13,20,21] and inhibit[22–24] catalysis. In all these cases, it remains unclear whether these dramatic effects stem from changes in the thermokinetic profile of the charge transfer steps, the chemical reaction steps or some combination of both. Yet, a detailed understanding of the factors that control the reaction condition dependence of the HER is a prerequisite for the rational design of improved catalysts and systems that operate under a wide array of reaction conditions.

Unfortunately, there currently exists a paucity of methods for discriminating the chemical and charge transfer contributions to overall HER catalytic efficiency and, correspondingly, their reaction condition dependence. This stems directly from the difficulty in quantifying the population, much less the chemical activity or reaction condition dependence of H_{OPD} in the catalytic cycle. As the key reactive H intermediates for the HER, H_{OPD} species exist at a thermodynamic excess relative to H_2 are thus are constantly being consumed under reaction conditions to release H_2. Although the precise chemical bonding environment remains contentious[25], H_{OPD} stands in stark contrast to strongly bound, under-potential deposited H, H_{UPD}, which form at potentials positive of the H^+/H_2 equilibrium potential, are persistent on noble metal surfaces and have been the subject of extensive thermodynamic and kinetic studies[11,13]. Spectroscopic studies have been able to observe and quantify H_{OPD} populations on Pt surfaces under steady-state catalysis conditions, but correlating the surface population of H_{OPD} with its chemical potential remains elusive[26,27]. Electrochemical transient methods have also been applied to quantify the activity of H_{OPD} on a variety of metals[3,28–31]. While valuable, this technique, which tracks the decay of the open circuit potential (OCP) following catalysis, inherently conflates double layer and adsorption contributions to electrode capacitance, making it hard to extract the H_{OPD} population or energetics unequivocally. This problem is compounded when comparing data across vastly different reaction conditions where additional contributions to capacitance cannot be excluded. Thus, improved strategies for quantifying the thermodynamics and kinetics of highly reactive H_{OPD} are needed to discriminate the relative contributions to medium-dependent HER kinetics.

The above challenges could be addressed if the critical H_{OPD} intermediates could be generated and delivered in a tuneable fashion to the catalyst surface from an external source rather than via charge transfer to the H_2 evolving interface. We postulate that independent control of the surface population of H_{OPD} would allow us to unambiguously generate a chemical overpotential without the need for charge transfer to the interface. This external delivery of H_{OPD} cannot be achieved on all noble metals; however, Pd is capable of intercalating H species which can diffuse rapidly within the bulk of the metal[32,33]. This property has been used to facilitate H_2 separations through thin Pd membranes[33–35]. Additionally, electrochemical polarization of a thin Pd membrane has been used to drive H-transport to a second medium to carry out hydrogenation reactions[36–43]. Thus, we envision that H-transport through a Pd membrane could be employed to externally control the surface population of H_{OPD} without charge transfer to the interface and to uncover how different reaction conditions affect the chemical and charge transfer overpotential contributions to HER catalysis.

Herein, we employ electrochemically driven H-insertion at one face (the H-pumping interface) of a thin Pd membrane to establish a tuneable, controlled H_{OPD} chemical potential at the opposite face (the analytical interface). We find, through a series of mechanistic studies, that the OCP of the analytical interface directly measures $\eta_{chemical}$ for H_2 evolution. We vary the rate of H-insertion to the analytical interface and correlate the shift in the OCP of the analytical interface with the rate of H_2 evolution at that interface to isolate the $\eta_{chemical}$-rate scaling for H_2 evolution catalysis. We further compare this scaling across a range of pH values, and in the presence of poisoning CO and promoting $Ni(OH)_2$. Remarkably, these studies reveal that across all the reaction conditions examined, the $\eta_{chemical}$-rate correlation plots overlay with a common scale factor of ~20 mV dec^{-1}. The data indicate that, upon normalizing to an equivalent $\eta_{chemical}$, the rate of net H–H recombination is remarkably insensitive to pH, or the presence of promoters or poisons. By super-imposing a small additional electrical polarization at the analytical interface on top of a high and fixed rate of H-insertion from the subsurface, we isolate the rate-overpotential scaling for the charge transfer step of HER at a nominally fixed H_{OPD} population. Unlike the $\eta_{chemical}$, we find that the $\eta_{charge\ transfer}$-rate scaling for the HER is dramatically impacted by electrolyte pH and the presence of promoters or poisons. Thus, we conclude that the reaction condition dependence of the HER on Pd catalysts results predominantly from the promotion or inhibition of the charge transfer kinetics between Pd and the electrolyte, rather than changes in the intrinsic rate of the chemical reaction steps involving surface H. Taken together, these findings reveal the importance of considering both the chemical and charge transfer contributions to HER overpotential, and how changing reaction conditions modulate these two components independently to define the overall reaction efficiency.

https://doi.org/10.1038/s41929-023-00943-2

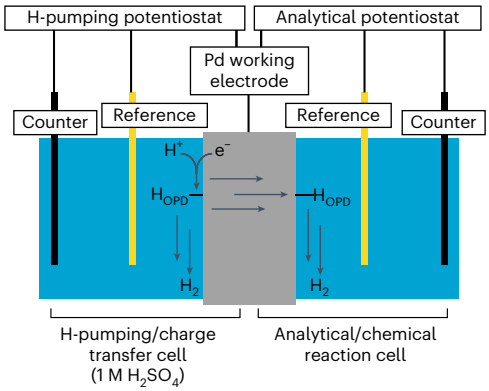

Fig. 2 | Illustration of the electrochemical double cell configuration. The electrochemical double cell consists of two electrochemical cells that are ionically isolated from one another despite sharing a common working electrode. In this electrochemical double cell configuration, proton reduction at the H-pumping interface generates H_{OPD}. The H_{OPD} at the H-pumping interface can then either spontaneously generate H_2 at the H-pumping interface, or diffuse into Pd and reform H_{OPD} at the analytical interface, where it is competent for H_2 release. Notably, charge transfer involved in H_{OPD} formation is isolated at the H-pumping interface, and is absent at the H_2-evolving analytical interface.

Results

Pd double cell generates H_{OPD} without direct charge transfer

To discriminate the chemical and charge transfer contributions to HER activity, we constructed a Pd membrane electrochemical double cell (Fig. 2; see the Methods for full experimental details)[44]. This configuration, which is also historically known as a Devanathan–Stachurski cell[32], consists of two distinct electrochemical cells separated by a Pd foil, which serves as the working electrode for both electrochemical cells, with separate counter and reference electrodes in each. Importantly, the pinhole-free nature of the Pd working electrode restricts the permeation of any liquids or electrolytes from one side to the other, thereby ionically isolating the two electrochemical cells[42]. Consequently, in this configuration, even though the working electrode is a single piece of metal and is contacted by two potentiostats, the current path for each electrochemical cell is distinct and, thus, no current flows from one face of the metal to the other. Consequently, each face of the common metal membrane can be independently polarized via charge transfer from the external circuit for that particular cell.

Most noble metal foils are completely impervious to ions and thus polarization of one face has no effect on the other. However, Pd can form bulk PdH_χ under reductive polarization in aqueous electrolytes, with the H fraction, χ, driven to higher values upon increased negative polarization, as given by the following electrochemical equilibrium:[32,42]

$$\chi H^+ + Pd + \chi e^- \rightleftharpoons PdH_\chi \quad (2)$$

Consequently, polarization of one Pd interface, termed the H-pumping interface, in an electrochemical double cell generates H_{OPD} species competent for H_2 release on the other, termed the analytical interface. Independently, the potential of the analytical interface of the Pd membrane can be measured and/or polarized by a second potentiostat, allowing us to probe the reactivity of H_{OPD} species in HER catalysis at the analytical interface at a steady-state population that has been orthogonally generated without net charge transfer at the analytical interface.

Using the above electrochemical double cell configuration, we tracked the OCP of the analytical interface upon polarizing the H-pumping interface. For this initial investigation, the electrolyte in the analytical cell was identical to the 1 M H_2SO_4 electrolyte in the H-pumping cell, and the analytical cell was kept under 1 atm of H_2. At a −1 mA cm^{-2} current density applied to the H-pumping interface, we observe a steady-state OCP at the analytical interface of −12 mV versus the RHE. This OCP value at the analytical interface shifts negatively in a linear fashion as the current passed at the H-pumping interface is increased logarithmically, reaching −47 mV versus RHE at a current density of −100 mA cm^{-2} at the H-pumping interface (Fig. 3a, red). Consistent with the OCP value being well negative of RHE, we observe vigorous H_2 evolution at the analytical interface (see below for quantitative analysis of H_2 release kinetics). The analytical interface also exhibits no history effects, reaching the same steady-state OCP value at a given current passed at the H-pumping interface irrespective of previous degrees of polarization at that interface. A linear fit to the data in Fig. 3a returns a slope of −17 mV change in OCP at the analytical interface per decade increase in current passed at the H-pumping interface. Upon termination of the polarization at the H-pumping interface (Fig. 3b, blue region), the OCP value decays towards more positive potentials as continued H_2 release lowers the interstitial and surface H populations, with analogous behaviour observed at the H-pumping interface (Supplementary Fig. 1). Importantly, when the Pd working electrode is replaced with a Pt foil, which does not intercalate or transport H, the OCP at the analytical interface is invariant with the amount of current passed and corresponding polarization at the opposite face of the Pt foil (Fig. 3a). Thus, under 1 atm of H_2, the Pt analytical interface remains pinned to the RHE irrespective of the current passed at the H-pumping interface. The foregoing data establish that increased reductive electrochemical polarization of the H-pumping interface leads to a systematic and progressive change in the open circuit electrochemical potential of the analytical interface as a direct result of H-transport through the Pd membrane.

The analytical interface OCP scales Nernstianly with pH

To determine the impact of the electrolyte pH on the OCP of the analytical interface, we set up an asymmetric electrochemical double cell. This asymmetric cell retained the same 1 M H_2SO_4 electrolyte in the H-pumping cell, but we systematically varied the pH and composition of the electrolyte in the analytical cell. This approach fixes a common reaction environment for generating reactive H species in the H-pumping cell, but allows us to probe H_2 evolution across a range of electrolyte conditions in the analytical cell. Importantly, the electrolyte composition only perturbs the interface between electrode and electrolyte, and should have no influence on the transport of reactive H species through the Pd membrane, which is a bulk property of the electrode. We stress that this orthogonalization is impossible to achieve in a typical electrochemical HER experiment at a single interface. We tracked the OCP of the analytical interface across a range of pH values, and find that the potential of the analytical interface shifts by 59 mV per pH unit (Fig. 3c). This slope is preserved across a range of current densities, ranging from −1 to −100 mA cm^{-2}, passed at the H-pumping interface (Fig. 3c). This Nernstian scaling with pH is also shown in Fig. 3d, where, across two orders of magnitude of current passed at the H-pumping interface, the OCP at the analytical interface remains largely unchanged versus the RHE reference (which by definition scales by 59 mV pH^{-1}). Additionally, the data in Fig. 3d highlight that across all pH conditions, the OCP measured at the analytical interface is driven well negative of the reversible hydrogen potential and that the −17 mV slope observed for the symmetrical double cell above is also preserved across the entire pH range. Furthermore, at circumneutral pH, the OCP at the analytical interface is independent of the buffer composition, with identical values recorded for formate/borate, formate/acetate and phosphate buffers (Fig. 3d). Together, the data evince that the electrochemical potential of the analytical interface scales in a purely Nernstian fashion with pH and is otherwise insensitive to the electrolyte composition.

The analytical interface OCP isolates $\eta_{chemical}$ for the HER

The above findings provide insight into the reactions that determine the potential of the analytical interface during steady-state

https://doi.org/10.1038/s41929-023-00943-2

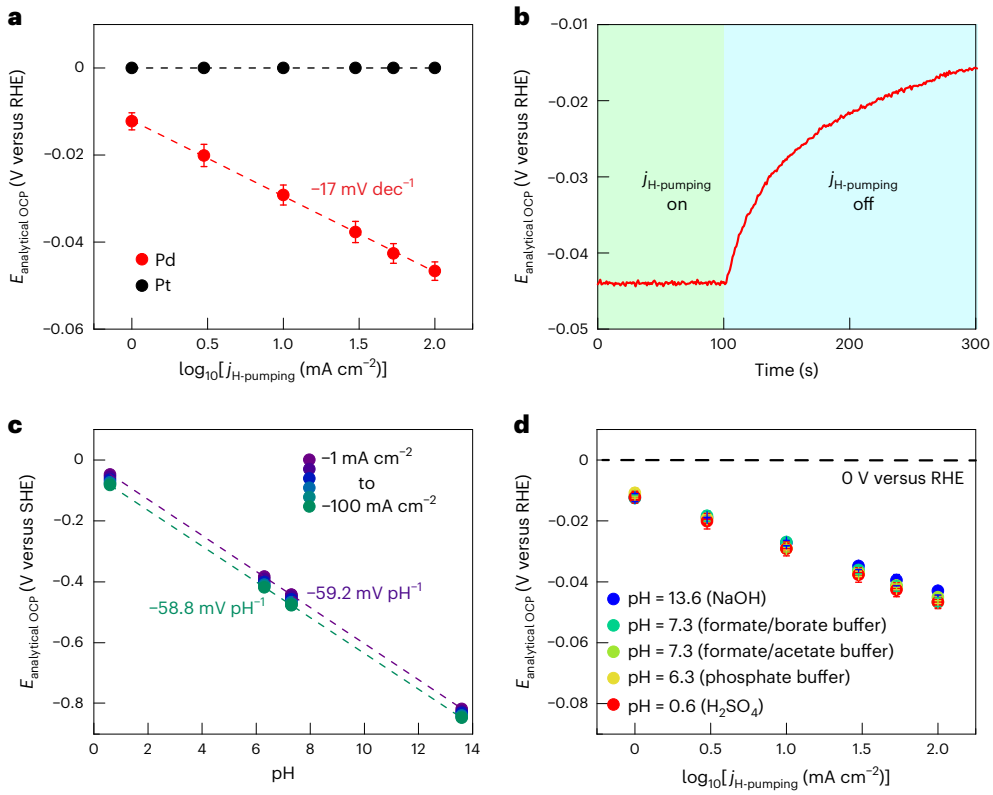

Fig. 3 | Polarization of the H-pumping interface affects the OCP behaviour of the analytical interface. a, OCP dependence of the analytical interface ($E_{analytical\ OCP}$) under galvanostatic polarization at the H-pumping interface ($j_{H\text{-}pumping}$) in a symmetric double cell configuration (1 M H_2SO_4 on both compartments), with Pd (red) and Pt (black) working electrodes. **b**, OCP of the analytical interface (red) under galvanostatic polarization of −100 mA cm^{-2} at the H-pumping interface ($j_{H\text{-}pumping}$ on, green region) and immediately after polarization is turned off ($j_{H\text{-}pumping}$ off, blue region). **c**, pH dependence of the analytical interface OCP versus the pH-independent standard hydrogen electrode (SHE) potential ($E_{analytical\ OCP}$) under galvanostatic polarizations ranging from −1 to −100 mA cm^{-2} at the H-pumping interface (error bars are smaller than the data point markers). **d**, OCP dependence of the analytical interface versus the pH-dependent RHE potential ($E_{analytical\ OCP}$) under galvanostatic polarization at the H-pumping interface ($j_{H\text{-}pumping}$) under different electrolyte pH conditions including 13.6 (blue), 7.3 (greens), 6.3 (yellow) and 0.6 (red) (some error bars are smaller than the data point markers). Data points are presented as mean values and error bars indicate standard deviations obtained from triplicate ($n = 3$) measurements.

H-pumping. Since the OCP is the potential at which zero net current passes, it reflects the potential at which the aggregate rate of anodic and cathodic charge transfer processes is balanced at the analytical interface. Thus, the foregoing data provide insight into the chemical participants in the charge transfer processes that set the OCP at the analytical interface. First, logarithmically increasing the current passed at the H-pumping interface leads to a linear shift of the analytical OCP on Pd to more negative values, an observation that is not retained on Pt (Fig. 3a). This implies that the interstitial H species, which are driven to higher fractions at higher H-pumping currents, are necessary for the induced spontaneous polarization of the analytical interface with the passage of reductive current at the H-pumping interface. Second, the Nernstian pH dependence (Fig. 3c,d) of the OCP indicates that the OCP is sampling a PCET process involving an equal number of electrons and protons. Third, the observation that the OCP values at the analytical interface are well negative of RHE across all pH values (Fig. 3d) and the observation of vigorous H_2 evolution at the analytical interface highlight that this interface is out of equilibrium relative to the H_2/H^+ electrochemical couple, and imply that the H species that set the OCP are H_{OPD}.

Two possible charge transfer reactions involving H_{OPD} can be envisioned: PCET to form and remove H_{OPD} (forward and reverse Volmer reaction) or PCET to interconvert H_{OPD} and H_2 (forward and reverse Heyrovsky reaction).

$$\text{Volmer step}: H^+ + Pd + e^- \rightleftharpoons Pd - H_{OPD} \quad (3)$$

$$\text{Heyrovsky step}: H^+ + Pd - H_{OPD} + e^- \rightleftharpoons Pd + H_2 \quad (4)$$

Thus, rigorously speaking, the OCP at the analytical interface samples a mixed potential of these two reaction steps. Importantly, electrons and protons are on the same side of both equilibria, and thus, irrespective of the relative contribution of each, the OCP will display a Nernstian scaling with pH. However, H_{OPD} is a product of the Volmer reaction step and is, instead, a reactant in the Heyrovsky reaction step. Increasing currents passed at the H-pumping interface and the correspondingly increased H_{OPD} population leads to a negative shift in the OCP, suggesting that the OCP value is dominated by the forward and reverse Volmer reactions. Furthermore, the minority contribution from the Heyrovsky step to the measured OCP is consistent with previous studies invoking a Volmer–Tafel mechanism as the primary pathway for H_2 evolution on Pd[7,31].

Taken together, the foregoing observations and analysis lead us to propose the following mechanistic model. Negative polarization at the H-pumping interface drives H-diffusion across the Pd membrane to form a non-equilibrium, steady-state H_{OPD} population at the analytical interface. This non-equilibrium H activity shifts the OCP via changes in the activity of H, a_H, in the potential-determining H_{OPD}/H^+ redox couple. Referencing to RHE accounts for proton activity, and therefore, the OCP at the analytical interface versus the RHE potential ($E_{analytical\ OCP}$ (V versus RHE)) provides a direct measure of the change in chemical potential of the surface H on Pd relative to its reference chemical potential at the RHE potential. Thus, given that the HER is a reductive process, the

$\eta_{chemical}$ can be calculated directly as the magnitude of the OCP deviation from the RHE potential:

$$\eta_{chemical} = -E_{analytical\,OCP}\ (\text{V versus RHE}) \quad (5)$$

(See Supplementary Note 2 for a detailed thermodynamic treatment of $\eta_{chemical}$ and $\eta_{charge\,transfer}$, and their relationship to the free energy changes of the Volmer and Tafel reaction steps.)

$\eta_{chemical}$-H_2 evolution rate scaling is pH-independent

The current passed at the H-pumping interface fractionates as H_2 evolution on both the H-pumping and analytical interfaces. Thus, the current passed at the H-pumping interface does not correspond to the rate of H_2 release at specifically the analytical interface where $\eta_{chemical}$ is measured. To establish a scaling relationship for the chemical overpotential with the rate of the HER, we used in-line gas chromatography analysis (Methods) to independently quantify the steady-state rate of H_2 evolution at the analytical interface. To facilitate comparisons, rates of H_2 evolution were converted to a current density (j) according to the following equation:

$$j = \upsilon_{H_2} \times nF \quad (6)$$

Here, υ_{H_2} is the rate of H_2 evolution at the analytical interface in mol s^{-1} cm^{-2}, n is 2 due to the two electrons in each H_2 molecule and F is the Faraday constant. Importantly, at open circuit, there is no net Faradaic charge transfer across the analytical interface, and thus the H_2 release at this interface must proceed via the net recombination of H_{OPD} species at the analytical interface:

$$2Pd - H_{OPD} \rightarrow 2Pd + H_2 \quad (7)$$

We note that this reaction could proceed by the combination of reverse Volmer and forward Heyrovsky steps. However, our studies below suggest that this is a minor contributor to the mechanism of H_2 release. Furthermore, independent studies that analysed OCP decay transients also concluded that Tafel recombination is the primary pathway for H_2 release on Pd[7,31].

We find that under all reaction conditions at the analytical interface, an increase in current passed at the H-pumping interface results in an increase in the steady-state rates of H_2 release at the analytical interface (see Supplementary Fig. 2 for permeation rates). Importantly, under equivalent currents passed at the H-pumping interface, the rate of H_2 evolution is also largely insensitive to changes in pH. Increasing the electrolyte pH at the analytical interface results in only a small attenuation in H_2 release rates at the analytical interface, 24.4 mA cm^{-2} in acid to 19.4 mA cm^{-2} in base under a constant −100 mA cm^{-2} current passed at the H-pumping interface (Supplementary Fig. 2). By combining all the H_2 release rates at different pH values with their corresponding measured $\eta_{chemical}$, we are then able to examine the pH dependence of the $\eta_{chemical}$-rate scaling for H_2 release (Fig. 4). We find that, across 13 pH units, the $\eta_{chemical}$-rate scaling for H_2 release at the analytical interface is pH-independent within error, with slopes ranging from 18–22 mV per decade and chemical overpotentials varying by <4 mV at equivalent H_2 release rates. Notably, increasing the membrane thickness from 25 to 100 μm leads to a largely unchanged scaling of H_2 release rate with $\eta_{chemical}$ (Supplementary Fig. 3), suggesting that these trends reflect the interfacial H–H recombination kinetics rather than the rate of H-transport through the Pd membrane. Interestingly, this measured slope falls below the 30 mV dec^{-1} slope predicted for H–H recombination controlled mechanisms with a Langmuirian isotherm for H_{OPD} adsorption (see Supplementary Note 3 for detailed derivation of the calculated 30 mV dec^{-1} Tafel slope for a Tafel rate-limited mechanism)[31]. The observed lower slope of 20 mV dec^{-1} could be explained by invoking an attractive non-Langmuirian H_{OPD} isotherm. For Pd, H-absorption into the bulk results in an expansion of the material, which has previously been invoked to decrease the enthalpy of subsequent H atom insertion and to result in an attractive isotherm for bulk Pd–H[45,46]. We posit that a similar phenomenon may be at play for surface H_{OPD} species. An attractive adsorption isotherm would cause the H_{OPD} surface concentration to rise in a non-Nernstian fashion (that is, <60 mV for a decade change in surface H concentration), leading to rates of H–H recombination that scale by less than the predicted 30 mV dec^{-1} expected for simple Langmuirian adsorption (Supplementary Note 4 and Supplementary Fig. 4). This finding motivates future operando spectroscopy and computational investigations to develop an atomistic picture of H_{OPD} adsorption across coverage.

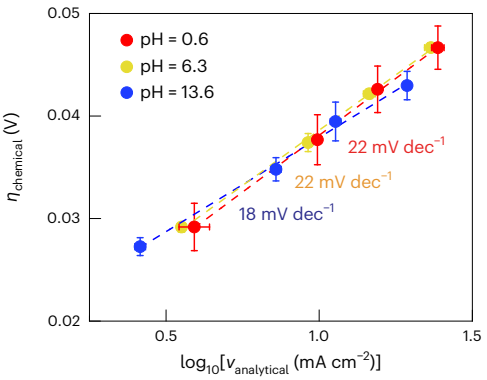

Fig. 4 | Rate scaling of H_2 release with chemical overpotential is pH-independent. The rate of H_2 release at the analytical interface ($\upsilon_{analytical}$) versus the chemical overpotential at that interface ($\eta_{chemical}$) under different pH conditions including 13.6 (blue), 6.3 (yellow) and 0.6 (red). Data points are presented as mean values and error bars indicate standard deviations obtained from triplicate (n = 3) measurements (some error bars are smaller than the data point markers).

The invariance of the rate of the Tafel reaction with electrolyte pH under equivalent chemical overpotentials stands in stark contrast to the ~100-fold decrease in the rate of the overall HER from acid to base reported on Pd[11,15]. In our system, H_2 release occurs in the absence of net Faradaic charge transfer, thereby excluding any contribution from the charge transfer overpotential. This finding suggests that the pH dependence of HER efficiencies in conventional electrochemical systems arises almost exclusively from kinetic differences in PCET charge transfer steps (quantified explicitly below) rather than changes in the chemical reactivity of surface H. Put simply, by supplying the key H_{OPD} intermediates from the bulk of the Pd membrane, rather than via PCET from solution, the pH-dependent efficiency losses in H_2 evolution catalysis are almost entirely eliminated.

Poisons and promoters do not affect $\eta_{chemical}$-rate scaling

Surface-bound poisons and promoters are known to dramatically influence the overall kinetics of HER catalysis on noble metals. For example, adsorption of CO serves to strongly attenuate HER activity[22–24], whereas islands of $Ni(OH)_2$ are known to promote HER rates in alkaline media[13,20,21]. However, it remains unclear whether these poisons and promoters augment HER rates via changes in the charge transfer kinetics, via changes to the kinetics of chemical reaction steps or by some combination of both. Using the double cell methodology described above, we isolate the impacts of CO and $Ni(OH)_2$ on the $\eta_{chemical}$-rate scaling for H_2 release.

To isolate the effect of CO, we introduced this poison to the analytical interface of the Pd electrochemical double cell with 1 M H_2SO_4 in both compartments. Under reductive polarization of −100 mA cm^{-2} at the H-pumping interface, the introduction of 1 atm of CO to the analytical cell resulted, as expected, in an attenuation of the H_2 release rate at

https://doi.org/10.1038/s41929-023-00943-2

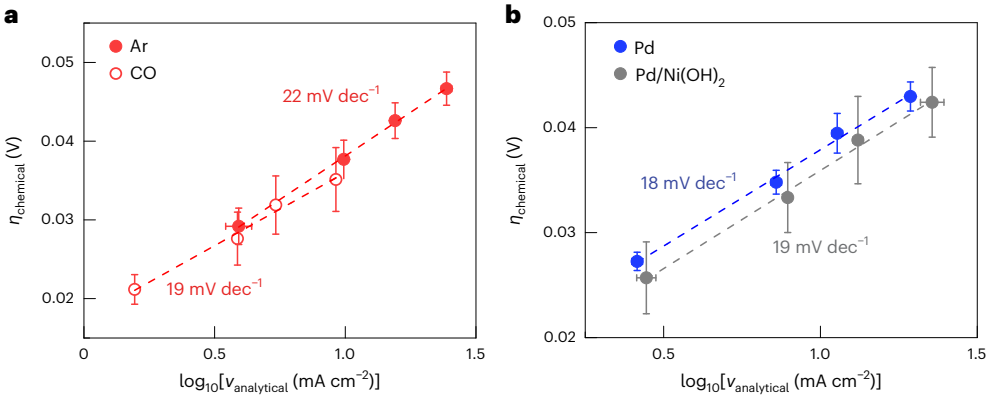

Fig. 5 | The rate scaling of H_2 release with chemical overpotential is unaffected by added CO or Ni(OH)$_2$. a, Rate of H_2 release at the analytical interface ($v_{analytical}$) versus the chemical overpotential at that interface ($\eta_{chemical}$) under an Ar atmosphere (solid red) and under a CO atmosphere (hollow red) (pH = 0.6). **b**, Rate of H_2 release at the analytical interface ($v_{analytical}$) versus the chemical overpotential at that interface ($\eta_{chemical}$) for both native Pd (blue) and Pd decorated with Ni(OH)$_2$ (grey) (pH = 13.6). Data points are presented as mean values and error bars indicate standard deviations obtained from triplicate ($n = 3$) measurements (some error bars are smaller than the data point markers).

the analytical interface, decreasing from 24.4 to 9.2 mA cm^{-2} (Supplementary Fig. 5b). This attenuation is consistent with CO binding to the analytical face to suppress H_2 release. Notably, the suppression in the H_2 release rate at the analytical interface with CO poisoning is also coupled to an attenuation of the $\eta_{chemical}$ at that interface, shifting from 47 mV to 35 mV (Supplementary Fig. 5a). This trend of both H_2 release rates and $\eta_{chemical}$ attenuating upon the addition of CO was observed across the entire range of currents sampled. Consequently, we find that the $\eta_{chemical}$-rate scaling for H_2 release is largely unaffected by the addition of CO (Fig. 5a). Thus, upon normalizing to an equivalent $\eta_{chemical}$ of, for example, 30 mV, the rates of H_2 release between the CO-poisoned and native Pd are largely unchanged at 4.74 and 4.29 mA cm^{-2}, respectively. Additionally, the CO-poisoned and native Pd display similar $\eta_{chemical}$-rate scaling factors for H_2 release of 19 and 22 mV dec^{-1}, respectively (Fig. 5a). These data suggest that although CO binds to Pd surface sites and hinders the formation of H_{OPD}, any interaction between CO and H_{OPD} has no substantial impact on the rate constant for H_{OPD} recombination to release H_2. Rather, the poisoning effect of CO on the overall HER stems principally from an inhibition of the charge transfer kinetics for interfacial PCET (see the 'Promoters or poisons affect the charge transfer kinetics' section below).

We also examined the effect of incorporating Ni(OH)$_2$ islands on the rate of H_2 release at the analytical interface. We deposited Ni(OH)$_2$ islands onto the analytical interface via galvanostatic oxidative electrodeposition (Methods). In contrast to the behaviour observed upon addition of CO, the incorporation of Ni(OH)$_2$ does not substantially attenuate the H_2 release rate at the analytical interface relative to the unmodified Pd interface (Supplementary Fig. 6b). Likewise, the addition of Ni(OH)$_2$ leads to no change in the OCP of the analytical interface within error (Supplementary Fig. 6a). Consistent with both of these observations, a plot of $\eta_{chemical}$ versus the rate of H_2 release at the analytical interface overlays for the samples with and without Ni(OH)$_2$ (Fig. 5b). These data evince that the presence of Ni(OH)$_2$ negligibly affects the $\eta_{chemical}$-rate scaling for H_2 release. Rather, the promoting effect of Ni(OH)$_2$ stems principally from an enhancement in the charge transfer kinetics for interfacial PCET (see below). This observation is consistent with the trends previously observed for H_{UPD} formation on Pt[13], which invoke that Ni(OH)$_2$ islands are able to lower the activation barrier for the Volmer reaction and have no impact on the energetics of the hydrogen intermediate or mechanism.

The foregoing studies highlight that both CO as a poison and Ni(OH)$_2$ as a promoter have minimal impact on the energetics associated with the chemical step of recombining H_{OPD} species to form H_2. Furthermore, similar to the above pH dependence study, the absence of net charge transfer from the interface entirely eliminates the typical HER efficiency changes observed upon introduction of poisons or promoters.

Fixing $\eta_{chemical}$ isolates charge transfer kinetics

The above data evince that the $\eta_{chemical}$-rate scaling for H_2 evolution is remarkably insensitive to changes in pH, the presence of surface poisons or the addition of surface promoters. Thus, these findings suggest that the strong reaction condition dependence of the overall HER reaction arises from changes in the charge transfer kinetics associated with the formation and removal of H_{OPD}. To test this hypothesis, we superimposed a small polarization at the analytical interface on top of a large background rate of H-pumping. Specifically, in all experiments, we set the current passed at the H-pumping interface to −100 mA cm^{-2}, which generates an elevated chemical overpotential at the analytical interface and corresponding steady-state rate of H_2 evolution in the analytical cell. During this background H_2 evolution process, we additionally polarized the analytical interface via electrical current flow from the external circuit in the analytical electrochemical cell. In the limit that the charge transfer rate at the analytical interface is small relative to the rate of H-transport from the opposite interface, the H_{OPD} population, and thus the $\eta_{chemical}$ at the analytical interface, should be minimally perturbed. By holding the $\eta_{chemical}$ roughly constant, the current potential relationship at the analytical interface should primarily sample the charge transfer kinetics. We apply this methodology to isolate and quantify the medium dependence of the charge transfer steps of hydrogen evolution catalysis.

$\eta_{charge\ transfer}$ changes with electrolyte pH

We quantified the current–$\eta_{charge\ transfer}$ relationship across a variety of pH values while holding the pH of the H-pumping interface constant at 1 M H_2SO_4. With the H-pumping interface polarized galvanostatically at −100 mA cm^{-2}, we recorded a series of stepped galvanostatic electrolyses in the analytical cell with current densities ranging from −3 to 3 mA cm^{-2} to generate Butler–Volmer (BV) plots of the charge transfer kinetics. Under these conditions, the background rate of H_2 evolution at the analytical interface from H-permeation across the membrane reaches ~23 mA cm^{-2}. Thus, the small additional current passed is expected to minimally perturb the H_{OPD} population and corresponding chemical overpotential. We note that extending the range of currents passed at the analytical interface to ±30 mA cm^{-2} did not appear to substantially impact the BV plots, and this is probably due

https://doi.org/10.1038/s41929-023-00943-2

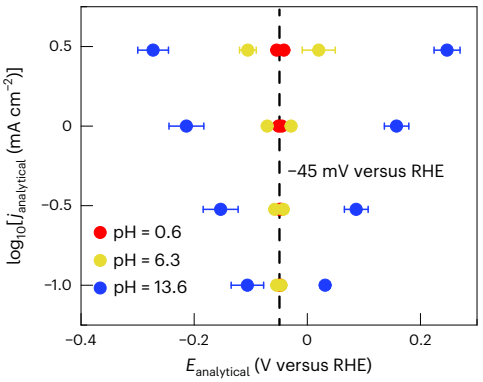

Fig. 6 | The charge transfer overpotential component is pH-dependent. BV behaviour for the hydrogen evolution/hydrogen oxidation reactions on the Pd analytical interface under a constant current density of −100 mA cm^{-2} passed at the H-pumping interface. Note that both the *x* and *y* axes refer to the potential measured ($E_{analytical}$) and the current density passed ($j_{analytical}$) at the analytical interface, respectively. Different pH conditions at the analytical interface include 13.6 (blue), 6.3 (yellow) and 0.6 (red). Data points are presented as mean values and error bars indicate standard deviations obtained from triplicate ($n = 3$) measurements (some error bars are smaller than the data point markers).

to the far greater overpotential-rate scaling observed for $\eta_{charge\ transfer}$ compared with $\eta_{chemical}$.

We first compared BV plots across acid, neutral and basic electrolyte conditions. Under all pH conditions, the BV plots converge in the limit of zero current to around −45 mV versus RHE, which is in close agreement with the chemical overpotential fixed by H-pumping to the analytical interface. Under acidic electrolyte conditions (Fig. 6), we observe charge transfer overpotentials of 5 and 7 mV for anodic and cathode current densities of 3 mA cm^{-2}, respectively. These charge transfer overpotentials increase with electrolyte pH, rising to 67 and 58 mV under near neutral conditions and increasing further to 294 and 226 mV under alkaline conditions (Fig. 6). Fitting these data to the BV equation (Supplementary Fig. 7) returns exchange current densities of 14, 7.6 and 0.21 mA cm^{-2} for solution pH values of 0.6, 6.3 and 13.6, respectively (see the Supplementary Methods for details of the fitting procedure). This dramatic attenuation in charge transfer kinetics contrasts with the invariance of the $\eta_{chemical}$-rate scaling across the same range of pH (Fig. 4). Notably, the ~70-fold attenuation in charge transfer kinetics between acid and base is similar to the ~100-fold rate change in overall HER kinetics between acidic and alkaline conditions on Pd[11,15], suggesting that the pH-dependent kinetics of HER accrue almost entirely from changes in the rate of charge transfer rather than changes in the rate of surface chemical reactions. The foregoing data on H_{OPD} also follow the same trend as previous reports studying strongly bound H_{UPD} species on Pt, which have reported substantial increases in the charge transfer resistance for the Volmer step with increasing electrolyte alkalinity[13]. Furthermore, the strong reaction condition dependence of the reverse Volmer reaction as shown in the anodic portion of the BV plot adds further insights into the H–H recombination pathway at the analytical interface. If H–H recombination at the analytical interface were to proceed via the combination of reverse Volmer and forward Heyrovsky steps, we would expect an analogous reaction-condition-dependent $\eta_{chemical}$ scaling with H_2 release to that observed for the reverse Volmer reaction. This is at odds with the reaction condition independence observed (Fig. 4), bolstering the notion that H_2 release at the analytical interface proceeds primarily through a Tafel recombination mechanism involving no charge transfer steps.

Promoters and poisons affect the charge transfer kinetics

Carbon monoxide is known to bind strongly to Pd surfaces and attenuate the rate of the HER. We applied the above methodology to isolate how the $\eta_{charge\ transfer}$-rate scaling for the HER changes upon addition of CO. Upon addition of 1 atm of CO to 1 M H_2SO_4 electrolyte, the charge transfer overpotential necessary to pass −3 mA cm^{-2} substantially increases from 7 mV to 260 mV (Fig. 7a). This also corresponds to a ~100-fold suppression in the rate of charge transfer at the same overpotential (Fig. 7a). In contrast, for the same 3 mA cm^{-2} rate of H_2 evolution on the analytical interface at OCP, we measure a chemical overpotential of ~30 mV both in the presence and absence of CO. These findings suggest that the presence of a CO poison serves to predominantly attenuate $\eta_{charge\ transfer}$ for forming H_{OPD}, but minimally impacts $\eta_{chemical}$.

Analogously, the deposition of islands of $Ni(OH)_2$ is known to promote HER in alkaline media on noble metals. We applied the above methodology to isolate the effect of $Ni(OH)_2$ on the charge transfer kinetics of the HER. The incorporation of $Ni(OH)_2$ onto Pd lowers the charge transfer overpotential necessary to pass 3 mA cm^{-2} from 226 to 94 mV and 294 to 154 mV for H_{OPD} generation and removal, respectively (Fig. 7b). Across the entire range of current densities sampled, the reduction in the charge transfer overpotential corresponded to a 6–10-fold enhancement in rate at a common overpotential (Fig. 7b), which is in line with the 5–8-fold activity enhancement previously reported for $Ni(OH)_2$-modified Pt surfaces[13,20]. Again, the strong effect that $Ni(OH)_2$ has on the charge transfer kinetics stands in stark contrast with the largely invariant $\eta_{chemical}$-rate scaling for H_2 release. Taken together, these data reveal that the HER promotion effects observed from the addition of $Ni(OH)_2$ on Pd serve to improve the charge transfer kinetics for HER without affecting the $\eta_{chemical}$-rate scaling for H_2 release.

Partitioning $\eta_{chemical}$ and $\eta_{charge\ transfer}$ for the HER

Aggregating the above data, we calculated the relative partitioning of the total overpotential into charge transfer and chemical contributions across all the conditions examined, at a common H_2 generation rate of 3 mA cm^{-2} (Fig. 8). At steady state, the rates of chemical and charge transfer steps in a Volmer–Tafel mechanism are balanced with each other and with the overall rate of H_2 generation, such that the H_{OPD} coverage is unchanged. The data in Figs. 4 and 5 provide the $\eta_{chemical}$, whereas the data in Figs. 6 and 7 provide the $\eta_{charge\ transfer}$ required for a given current density of H_2 evolution. At pH 0.6 we find that the $\eta_{chemical}$ (30 mV) is substantially greater than the $\eta_{charge\ transfer}$ (7 mV) (Fig. 8). This adds nuance to the general mechanistic consensus that the chemical step for H–H recombination limits the rate of HER catalysis in acidic aqueous media[8,13,47]. Indeed, previous work has reported Tafel slopes as low as 30 mV dec^{-1} for the overall HER on Pd in acid[47]. Such low Tafel slopes have been interpreted as a Volmer–Tafel mechanism with a rate-limiting Tafel step, implying that all the overpotential for the HER in acid arises from chemical overpotential with no charge transfer overpotential contribution. Our data suggest a more nuanced explanation: both charge transfer (Volmer) and chemical reaction (Tafel) steps contribute to the overpotential of HER in acid, and the 20 mV dec^{-1} scaling of the latter (Fig. 4) combines with the charge transfer overpotential contribution to give rise to the 30 mV dec^{-1} Tafel slope for the overall reaction. Indeed for the H-pumping interface, where both charge transfer and chemical overpotentials contribute, we too observe a Tafel slope of 30 mV dec^{-1} (Supplementary Fig. 8).

The charge transfer overpotential contribution to the overall HER is far more amplified at elevated pH. At pH 6.3 the $\eta_{chemical}$ constitutes a minority fraction of the overall overpotential due to the substantial attenuation in charge transfer kinetics. This trend becomes even more pronounced at pH 13.6, where the 225 mV charge transfer overpotential dwarfs the measured 28 mV chemical overpotential (Fig. 8). The invariance of the $\eta_{chemical}$ across the entire pH range combined with the large change in the $\eta_{charge\ transfer}$ provides the clearest evidence to date that HER efficiency losses stem predominantly, if not exclusively, from changes in charge transfer kinetics. Numerous previous studies have examined the impacts of electrolyte cations and buffering species on HER kinetics[14,16–19,21], and we posit that the methodology developed here can

https://doi.org/10.1038/s41929-023-00943-2

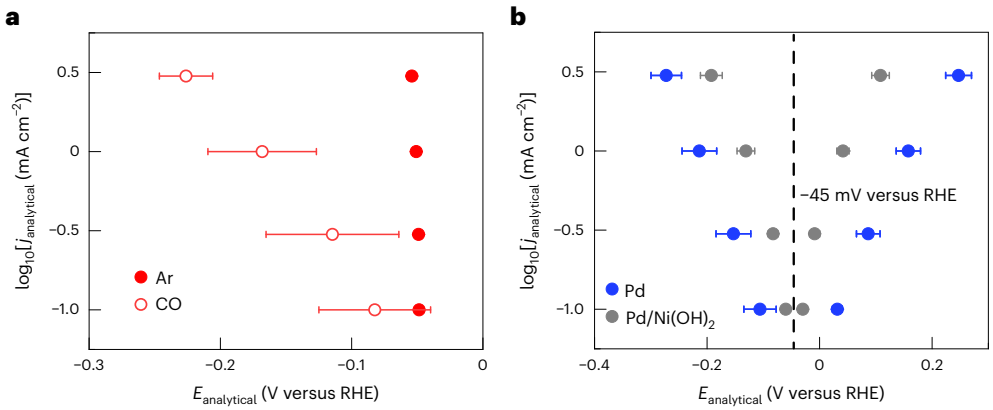

Fig. 7 | The charge transfer overpotential component is affected by added CO and Ni(OH)$_2$. a, BV behaviour for HER on the Pd analytical interface under a constant current density of −100 mA cm^{-2} passed at the H-pumping interface for Pd under both an Ar (solid red) and a CO atmosphere (hollow red) (pH = 0.6). **b**, BV behaviour for HER on the Pd analytical interface under a constant current density of −100 mA cm^{-2} passed at the H-pumping interface for both native Pd (blue) and Pd decorated with Ni(OH)$_2$ (grey) (pH = 13.6). Data points are presented as mean values and error bars indicate standard deviations obtained from triplicate (n = 3) measurements (some error bars are smaller than the data point markers).

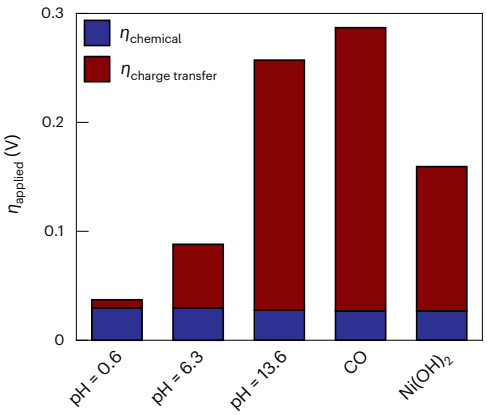

Fig. 8 | Contributions of chemical and charge transfer overpotentials for hydrogen catalysis under different reaction conditions. The chemical (blue) and charge transfer (red) overpotential components for passing 3 mA cm^{-2} of HER current density on Pd under different reaction conditions.

be readily extended to isolate the relative chemical and charge transfer overpotential contributions in each case. Furthermore, whereas these findings provide direct insight into the thermochemistry of H_{OPD} under HER conditions, they do not provide a measure of the surface coverage of H_{OPD}. Indeed, these studies could be coupled with operando infrared spectroscopy of the analytical interface to connect the surface population with the chemical potential of H_{OPD}, thereby providing a direct measure of the isotherm for kinetically competent H intermediates for the HER.

Even under acidic conditions, the addition of CO causes a remarkable attenuation in charge transfer kinetics, with an additional 250 mV of charge transfer overpotential necessary to pass 3 mA cm^{-2} of HER current density. However, this change does not translate into any increase in the $\eta_{chemical}$ for H–H recombination. Previous studies have examined co-adsorbate interactions between surface CO and surface H, but have led to conflicting conclusions suggesting both cooperative and inhibitory interactions[48–52]. While our finding would be consistent with a model in which adsorbed CO and H_{OPD} interact minimally, the data may also imply that CO preferentially binds to the surface active site for the Volmer reaction and that distinct sites carry out H–H recombination. The methodology we develop here sets the stage for more detailed mechanistic and surface structural studies on the interplay of surface CO and H during HER catalysis. Expanding our analysis to an HER promoter, we find that under basic conditions, the high native charge transfer overpotential for the HER can be reduced on Pd by ~100 mV by depositing islands of Ni(OH)$_2$ on the surface. However, similar to the addition of CO, Ni(OH)$_2$ does not appreciably alter the $\eta_{chemical}$-rate scaling for H_2 release. This observation is consistent with previous studies on H_{UPD} formation, and how Ni(OH)$_2$ islands on Pt are able to facilitate PCET for H_{UPD} formation, but have only nominal effects on the energetics and reactivity of surface H[13]. Taken together, these findings highlight the power of using the electrochemical double cell analysis to discriminate the chemical and charge transfer contributions to HER catalysis.

Conclusions

This study reveals the importance of considering both the chemical and charge transfer overpotential components that make up electrocatalysis occurring at electrode interfaces. For the case of the HER, both the elevated, out-of-equilibrium chemical activity of H_{OPD} and the polarization necessary to drive charge transfer generate individual chemical and charge transfer overpotential components, respectively, to the aggregate overpotential. To isolate how changing reaction conditions independently tune both these components to affect overall HER efficiencies, we orthogonalize the delivery of H_{OPD} to a Pd surface using an electrochemical double cell system. In doing so, we are able to generate H_{OPD} without charge transfer to the interface of interest, and thus isolate the chemical overpotential for the HER. We are also able to further isolate the charge transfer overpotential component for the HER by maintaining an elevated chemical overpotential and further polarizing the Pd interface of interest.

Our principal findings can be summarized as follows. In all reaction conditions examined, the chemical overpotential-rate scaling for H_2 release is largely unaffected by reaction conditions. Thus, by supplying the key H_{OPD} intermediate for HER without charge transfer at the interface, the reaction condition dependence of H_2 generation is eliminated. Instead, the reaction condition dependence of overall HER catalysis stems entirely from changes in the charge transfer overpotential, which is dramatically impacted. Bifurcating the overall overpotential into chemical and charge transfer components can guide catalyst design. For example, in acidic media, where PCET is rapid and the charge transfer overpotential is a minor component, the surface structure of the catalyst should be the primary target for optimization to reduce the chemical overpotential component. In contrast, under conditions where the charge transfer overpotential dominates, such as

when poisoned by CO or when in alkaline media, design efforts should centre on tuning the electrolyte and surface promoter composition to enhance PCET kinetics. By highlighting how different reaction conditions independently affect the chemical and charge transfer overpotential contributions to electrocatalysis occurring at electrode interfaces, these studies aim to reimagine future directed design of catalytic systems for improved efficiencies in electrochemical transformations.

Methods

General electrochemical methods

BioLogic VMP 16-channel potentiostats were used for all electrochemical experiments. Ag/AgCl reference electrodes were obtained from BASi (3 M NaCl) and eDAQ (leakless, ET069). Pt/C (0.5 mg cm^{-2}) gas diffusion electrodes (GDEs) were obtained from the Fuel Cell Store. Alicat mass flow controllers were used to control gas flow rates to each electrochemical compartment. In all experiments, each solution was sparged with Ar at 10 sccm for at least 30 min before any polarization to remove dissolved oxygen from the electrolyte. Electrochemical studies were carried out using custom-built, gas-tight, glass H-cell parts. All experiments involved the use of two different three-electrode setups, with one comprising the H-pumping cell and the other comprising the analytical cell. The Pd foil membrane acted as the working electrode for both three-electrode setups. The geometric area of the Pd foil was controlled by the o-ring gasket of the H-cell joint and was 1 cm^2. All current densities are normalized to this geometric footprint rather than the electrochemically active surface area. A Pt mesh or Pd foil was used as counter electrodes (both of which returned identical results).

Three electrochemical cell configurations were used (Supplementary Fig. 9). The first configuration (Supplementary Fig. 9a) contained two separated three-electrode cells (the H-pumping and analytical cells) with a common Pd membrane working electrode. For each three-electrode cell, the working (Pd) and counter (Pd or Pt) electrodes were not separated by a membrane separator. The second configuration (Supplementary Fig. 9b) contained a Nafion 117 membrane separating working and counter compartments of the H-pumping cell; working and counter electrodes remained unseparated in the analytical cell. The third configuration (Supplementary Fig. 9c) contained membrane separators between working and counter compartments in both the H-pumping and analytical cells. Nafion was employed as the separator when the electrolyte was acidic and neutral, and Selemion AMV-N was employed for alkaline electrolytes. It was found that the inclusion of a membrane separator had no appreciable effect on the electrochemical response of the system, and, as such, most of the data were collected using no membrane separators in either the H-pumping or analytical cells (configuration in Supplementary Fig. 9a). All cell components were cleaned before use by immersion in concentrated sulfuric acid for at least 1 h, followed by copious rinsing with Milli-Q water and drying under flowing Ar.

During all experiments, the electrochemical double cell was placed on a VWR 200 Rocking Platform Shaker set to rock at setting 2 to dislodge H_2 bubbles generated at the Pd interface during electrolysis.

In-line gas quantitation

H_2 gas emanating from the analytical compartment was quantified by in-line gas chromatography (GC) using an SRI Instruments Multi-Gas Analyzer, Model 8610C, equipped with a thermal conductivity detector and a 2 m ShinCarbon (Restek) column. For experiments containing CO, in-line H_2 quantitation was conducted using an in-line gas chromatograph (SRI Instruments, Multi-Gas Analyzer, Model 8610C) equipped with a thermal conductivity detector and two MolSieve 13X and Hayesep D columns connected in series.

Palladium preparation

Pd foil electrodes were cleaned and palladized before use in the electrochemical double cell. For the cleaning step, the Pd membrane double cell was assembled, with a 1 cm^2 geometric surface area of Pd exposed to the electrolyte in the analytical and H-pumping cells. Both sides of the Pd foil were first simultaneously cleaned by cyclic voltammetry cycling in 1 M H_2SO_4 electrolyte under a continuous 10 sccm Ar sparge. Cyclic voltammetry cycling commenced at the OCP scanning negative at 50 mV s^{-1} scan rate. The electrode was cycled between 0.1 and 1.1 V versus Ag/AgCl (3 M NaCl) for 100 cycles. This cleaning procedure was conducted using a Pt mesh or Pd foil counter electrode. Both sides of the foil were then thoroughly washed with Milli-Q water (without disassembling the double cell).

Following cleaning by cyclic voltammetry cycling, the Pd foil was retained in the same electrochemical double cell, and both sides of the Pd working electrode were palladized. A fresh 15.9 mM $PdSO_4$ solution in 1 M HCl was used for each palladization preparation. An Ag/AgCl (3 M NaCl) electrode and a Pt mesh or Pd foil were used as the reference and counter electrodes, respectively, in each compartment. The H-pumping and analytical cell compartments were each filled with 10 mL of the palladization solution, and each face of the Pd working electrode was simultaneously polarized potentiostatically to −0.2 V versus Ag/AgCl (3 M NaCl) without resistance (iR) compensation until 7.38 C cm^{-2} of charge. The palladization procedure was carried out under a continuous 10 sccm Ar sparge. The palladized Pd foil was then thoroughly washed with Milli-Q water (without disassembling the double cell) and dried in flowing Ar.

Electrochemical deposition of $Ni(OH)_2$ onto Pd

The analytical compartment was charged with 10 mL of 0.005 M $NiCl_2{\cdot}6H_2O$ electrolyte. The palladized Pd foil was then galvanostatically polarized at +400 μA for 15 min in a two-electrode setup with a Pt mesh as the counter electrode. The foil was then thoroughly washed with Milli-Q water (without disassembling the double cell) and dried in flowing Ar.

Determining $\eta_{chemical}$-rate scaling for H_2 release

Measurements of the OCP at the analytical interface at varying currents passed at the H-pumping interface were performed with the following setup: For the H-pumping cell, an Ag/AgCl (3 M NaCl) was used as the reference electrode and a Pt mesh or Pd foil was used as the counter electrode. In all experiments, the electrolyte used in the H-pumping cell was 1 M H_2SO_4. The H-pumping cell was also sparged with 10 sccm Ar, although replacing the gas with H_2 did not affect any of the measurements. For the analytical cell, a hanging strip Pt GDE was used as the reference electrode (which operates as an RHE when under an H_2 atmosphere) and either a Pt mesh or Pd foil was used as the counter electrode. The analytical cell was sparged with 10 sccm H_2, although no difference in potential between the additional reference and the Pd working electrode was observed when H_2 was replaced with Ar (however, the Pt GDE would no longer be capable of acting as a reference electrode). Electrolytes used in the analytical cell included 1 M H_2SO_4 (pH = 0.6), 1 M sodium hydroxide (pH = 13.6), 1 M lithium hydroxide (pH = 13.6), 0.5 M sodium formate + 0.5 M sodium borate + 1 M sodium perchlorate buffer (pH = 7.3), 0.5 M sodium acetate + 0.5 M sodium borate + 1 M sodium perchlorate buffer (pH = 7.3) and 1 M sodium phosphate + 1 M sodium perchlorate buffer (pH = 6.3) (Fig. 3). All experiments involving $Ni(OH)_2$ were conducted in 1 M sodium hydroxide (pH = 13.6) (Supplementary Fig. 6a).

For measurement of the OCP of the analytical interface, the H-pumping interface was galvanostatically polarized at current densities ranging from −1 to −100 mA cm^{-2}. During each galvanostatic electrolysis, the OCP was recorded in the analytical cell. Galvanostatic polarization on the H-pumping cell was held until the OCP at the analytical interface reached a stable value, which took between 1 to 20 min. These steady-state open circuit values at the analytical interface provided the *y*-axis data points in Fig. 3a and Supplementary Figs. 5a and 6a.

For measurements of the H_2 permeation rate at the analytical interface under galvanostatic polarization at the H-pumping interface, the following setup was employed: For the H-pumping cell, an Ag/AgCl (3 M NaCl) was used as the reference electrode and a Pt mesh or Pd foil was used as the counter electrode. A three-compartment cell was used such that the working and counter electrodes of the H-pumping cell were separated by a Nafion membrane. The electrolyte used was 1 M H_2SO_4 in all experiments. For the analytical cell, an Ag/AgCl (3 M NaCl in acid and neutral electrolytes, leakless in alkaline electrolytes) was used as the reference electrode and either a Pt mesh or Pd foil was used as the counter electrode. Both cells were sparged independently with Ar at 10 sccm. The current density at the H-pumping interface ranged from −10 to −100 mA cm^{-2}, and the analytical interface was held at the OCP for the duration of the experiment. The outflow of the analytical compartment was analysed via gas chromatography to measure the amount of H_2 that permeated across the Pd membrane. In each experiment, galvanostatic electrolysis at the H-pumping interface was maintained for 30 min, which afforded enough time to reach a steady-state H_2 evolution rate at the analytical interface as judged by a stable gas chromatography response. The recorded OCP values at the analytical interface were converted to the RHE scale using the following equation, $E_{RHE} = E_{Ag/AgCl} + 0.210\ V + 0.059\ V \times pH$, and were unchanged from the potentials measured under an H_2 atmosphere using the RHE reference electrode in the experiments mentioned above.

H_2 evolution in the analytical cell compartment was measured using an in-line gas chromatograph and detected using the equipped thermal conductivity detector. A 2 m ShinCarbon (Restek) column with an isothermal temperature programme (165 °C) and Ar carrier gas (UHP, Airgas, 20 psi) were used to separate H_2 from possible contaminant gasses (O_2 or N_2), which were not observed in the effluent from either cell. GC traces were collected every 3 min from a 0.5 mL sample loop injection. The concentration of H_2 was determined via integrated peak area via a calibration curve. The partial current density for H_2 was calculated using the following equation:

$$j_i = c_i \times n_i \times F \times V_{gas} \times \frac{P}{RT} \times \frac{1}{A} \quad (8)$$

where c_i is the gas chromatography detected product in ppm, n_i is the electron stoichiometry for the H_2 product, 2, F is Faraday's constant (96,485 C mol^{-1}), V_{gas} is the substrate gas flow rate (10 sccm in all cases), P is the pressure in the cell (1 atm), A is the sample surface area, R is the gas constant and T is temperature.

To establish a chemical overpotential-rate scaling for H_2 release, the deviation of the OCP from RHE at the analytical interface (measured from OCP experiments under both an H_2 and Ar atmosphere) was plotted against the log rate of H_2 release measured at that same interface. Chemical overpotential-rate scaling for H_2 release relationships were obtained for electrolytes in the analytical cell including 1 M H_2SO_4 acid (pH = 0.6), 1 M sodium hydroxide (pH = 13.6) and 1 M sodium phosphate + 1 M sodium perchlorate buffer (pH = 6.3). The foregoing procedure generated the data in Fig. 4. All experiments involving $Ni(OH)_2$ were conducted in 1 M NaOH and generated the data in Fig. 5b.

Determining $\eta_{chemical}$ -rate scaling for H_2 release with CO

For studies that examined the effect of CO poisoning on the Pd membrane double cell, slight modifications to the above method were applied: The electrolyte used in both the H-pumping and analytical cells was 1 M H_2SO_4. For the H-pumping cell, an Ag/AgCl (3 M NaCl) was used as the reference electrode and a Pt mesh or Pd foil was used as the counter electrode. The H-pumping cell was sparged with 10 sccm Ar for the duration of the experiment. For the analytical cell, an Ag/AgCl (3 M NaCl) was used as the reference electrode and either a Pt mesh or Pd foil was used as the counter electrode. The analytical cell was initially sparged with 10 sccm Ar, and switched to 20 sccm CO during the course of the experiment. To measure the chemical overpotential, galvanostatic polarization with current densities ranging from −1 to −100 mA cm^{-2} was performed at the H-pumping cell, and the OCP was measured on the analytical cell (Supplementary Fig. 5a). Galvanostatic polarization on the H-pumping cell was held until the open circuit response stabilized, which took anywhere from 1 to 20 min. The recorded OCP values at the analytical interface were converted to the RHE scale using the following equation, $E_{RHE} = E_{Ag/AgCl} + 0.210\ V + 0.059\ V \times pH$.

The same cell setup was used to measure H_2 permeation rates at the analytical interface under CO poisoning conditions. H_2 was measured using an in-line gas chromatograph and detected using the equipped thermal conductivity detector. Both cells were initially sparged independently with Ar at 10 sccm. Then, the sparge gas in the analytical cell was switched to CO at 20 sccm. The current density at the H-pumping interface ranged from −10 to −100 mA cm^{-2}, and the analytical interface was held at OCP for the duration of the experiment. The outflow of the analytical compartment was analysed via gas chromatography to measure the amount of H_2 permeation across the Pd membrane. The partial current density for H_2 was calculated using the same equation as above. Each H-pumping current was maintained for 40 min, which yielded a stable gas chromatography response for H_2 detection.

To establish a chemical overpotential-rate scaling for H_2 release with CO poisoning, the deviation of the OCP from RHE at the analytical interface was plotted against the log rate of H_2 release measured at that same interface to produce the plot in Fig. 5a.

Isolating $\eta_{charge\ transfer}$ for the HER (with and without CO)

For experiments isolating the charge transfer overpotential component for H_2 catalysis (Figs. 6 and 7), simultaneous polarization of both the H-pumping and analytical interfaces of the Pd membrane was performed. In all experiments, the current density at the H-pumping interface was maintained at −100 mA cm^{-2}. Simultaneously, current was passed at the analytical interface. For experiments that did not involve CO (Figs. 6 and 7b), the analytical compartment was sparged with H_2 at 10 sccm, and a Pt GDE was used as the reference electrode. Current densities at the analytical interface ranged from −30 to 30 mA cm^{-2}, with galvanostatic polarization held until the potential at the analytical interface reached steady state (between 5 and 10 min). For unmodified Pd electrodes, the electrolytes used in the analytical cell included 1 M H_2SO_4 acid (pH = 0.6), 1 M sodium hydroxide (pH = 13.6) and 1 M sodium phosphate + 1 M sodium perchlorate buffer (pH = 6.3) and produced the data in Fig. 6. All experiments involving $Ni(OH)_2$-modified Pd were conducted in 1 M sodium hydroxide (pH = 13.6) and produced the data in Fig. 7b. For experiments that involved CO, the analytical compartment was sparged with CO at 20 sccm and an Ag/AgCl (3 M NaCl) was used as a reference electrode. Current densities at the analytical interface ranged from −3 to 0 mA cm^{-2}. Oxidative currents could not be sampled under CO as measured potentials were unstable and did not reach steady state. This procedure generated the data in Fig. 7a.

Fitting of double polarization BV plots was performed in MATLAB (v.2021b) via a non-linear least squares method. The experimental current density (j) and potential (E) data were fit to the logarithm of the absolute value of the BV equation:

$$\log_{10}|j| = \log_{10}\left|j_0 e^{\alpha\frac{F(E-E_0)}{RT}} - j_0 e^{-(1-\alpha)\frac{F(E-E_0)}{RT}}\right| \quad (9)$$

where F is Faraday's constant, R is the ideal gas constant and T is the temperature (300 K). The equilibrium potential (E_0), exchange current density (j_0) and the symmetry factor (α) were parameters determined from the fitting procedure. When the current density is large or more polarized, it is convoluted by a non-negligible shift in chemical overpotential at steady state. To minimize the effect of this convolution on the fit, the data points were weighted by the reciprocal of the absolute value

of *j*. The average of the least polarized anodic and cathodic potentials was used as the starting value for the equilibrium potential. A symmetry factor of 0.5 and current density of 1.0 nA cm^{-2} were used for the other starting values. Data fitting was used to produce the plot in Supplementary Fig. 7.

Data availability

The source data that support the findings of this study are available from the corresponding author on reasonable request.

References

1. Seh, Z. W. et al. Combining theory and experiment in electrocatalysis: insights into materials design. *Science* **355**, eaad4998 (2017).
2. Quaino, P., Juarez, F., Santos, E. & Schmickler, W. Volcano plots in hydrogen electrocatalysis – uses and abuses. *Beilstein J. Nanotechnol.* **5**, 846–854 (2014).
3. Tilak, B. V. & Conway, B. E. Analytical relations between reaction order and Tafel slope derivatives for electrocatalytic reactions involving chemisorbed intermediates. *Electrochim. Acta* **37**, 51–63 (1992).
4. Conway, B. E. & Liu, T. C. Behaviour of surface intermediate states in anodic O_2 evolution electrocatalysis at Co_3O_4 on Ni and Ti substrates. *Ber. Bunsenges. Phys. Chem.* **91**, 461–469 (1987).
5. Bockris, J. O. & Potter, E. C. The mechanism of the cathodic hydrogen evolution reaction. *J. Electrochem. Soc.* **99**, 169–186 (1952).
6. Shinagawa, T., Garcia-Esparza, A. T. & Takanabe, K. Insight on Tafel slopes from a microkinetic analysis of aqueous electrocatalysis for energy conversion. *Sci. Rep.* **5**, 13801 (2015).
7. Enyo, M. & Maoka, T. The overpotential components on the palladium hydrogen electrode. *J. Electroanal. Chem. Interfacial Electrochem.* **108**, 277–292 (1980).
8. Enyo, M. & Maoka, T. The hydrogen electrode reaction mechanism on palladium and its relevance to hydrogen sorption. *Surf. Technol.* **4**, 277–290 (1976).
9. Green, J. A. S. & Lewis, F. A. Overvoltage component at palladized cathodes of palladium and palladium alloys prior to and during bubble evolution. *Trans. Faraday Soc.* **60**, 2234–2243 (1964).
10. Sheng, W. et al. Correlating hydrogen oxidation and evolution activity on platinum at different pH with measured hydrogen binding energy. *Nat. Commun.* **6**, 5848 (2015).
11. Zheng, J., Sheng, W., Zhuang, Z., Xu, B. & Yan, Y. Universal dependence of hydrogen oxidation and evolution reaction activity of platinum-group metals on pH and hydrogen binding energy. *Sci. Adv.* **2**, 3 (2016).
12. Chen, X., McCrum, I. T., Schwarz, K. A., Janik, M. J. & Koper, M. T. M. Co-adsorption of cations as the cause of the apparent pH dependence of hydrogen adsorption on a stepped platinum single-crystal electrode. *Angew. Chem. Int. Ed.* **56**, 15025–15029 (2017).
13. Ledezma-Yanez, I. et al. Interfacial water reorganization as a pH-dependent descriptor of the hydrogen evolution rate on platinum electrodes. *Nat. Energy* **2**, 17031 (2017).
14. Jung, O., Jackson, M. N., Bisbey, R. P., Kogan, N. E. & Surendranath, Y. Innocent buffers reveal the intrinsic pH- and coverage-dependent kinetics of the hydrogen evolution reaction on noble metals. *Joule* **6**, 476–493 (2022).
15. Durst, J. et al. New insights into the electrochemical hydrogen oxidation and evolution reaction mechanism. *Energy Environ. Sci.* **7**, 2255–2260 (2014).
16. Jackson, M. N., Jung, O., Lamotte, H. C. & Surendranath, Y. Donor-dependent promotion of interfacial proton-coupled electron transfer in aqueous electrocatalysis. *ACS Catal.* **9**, 3737–3743 (2019).
17. Goyal, A. & Koper, M. T. M. The interrelated effect of cations and electrolyte pH on the hydrogen evolution reaction on gold electrodes in alkaline media. *Angew. Chem. Int. Ed.* **60**, 13452–13462 (2021).
18. Monteiro, M. C. O., Goyal, A., Moerland, P. & Koper, M. T. M. Understanding cation trends for hydrogen evolution on platinum and gold electrodes in alkaline media. *ACS Catal.* **11**, 14328–14335 (2021).
19. Huang, B. et al. Cation- and pH-dependent hydrogen evolution and oxidation reaction kinetics. *JACS Au* **1**, 1674–1687 (2021).
20. Subbaraman, R. et al. Enhancing hydrogen evolution activity in water splitting by tailoring Li^+-$Ni(OH)_2$-Pt interfaces. *Science* **334**, 1256–1260 (2011).
21. McCrum, I. T. & Koper, M. T. M. The role of adsorbed hydroxide in hydrogen evolution reaction kinetics on modified platinum. *Nat. Energy* **5**, 891–899 (2020).
22. Leiva, E. P. M., Santos, E. & Iwasita, T. The effect of adsorbed carbon monoxide on hydrogen adsorption and hydrogen evolution on platinum. *J. Electroanal. Chem. Interfacial Electrochem.* **215**, 357–367 (1986).
23. Ji, S. G., Kim, H., Park, C., Kim, W. & Choi, C. H. Underestimation of platinum electrocatalysis induced by carbon monoxide evolved from graphite counter electrodes. *ACS Catal.* **10**, 10773–10783 (2020).
24. Rodriguez, P., Feliu, J. M. & Koper, M. T. M. Unusual adsorption state of carbon monoxide on single-crystalline gold electrodes in alkaline media. *Electrochem. Commun.* **11**, 1105–1108 (2009).
25. Zeradjanin, A. R., Grote, J.-P., Polymeros, G. & Mayrhofer, K. J. J. A critical review on hydrogen evolution electrocatalysis: re-exploring the volcano-relationship. *Electroanalysis* **28**, 2256–2269 (2016).
26. Kunimatsu, K., Senzaki, T., Samjeské, G., Tsushima, M. & Osawa, M. Hydrogen adsorption and hydrogen evolution reaction on a polycrystalline Pt electrode studied by surface-enhanced infrared absorption spectroscopy. *Electrochim. Acta* **52**, 5715–5724 (2007).
27. Zhu, S., Qin, X., Yao, Y. & Shao, M. pH-dependent hydrogen and water binding energies on platinum surfaces as directly probed through surface-enhanced infrared absorption spectroscopy. *J. Am. Chem. Soc.* **142**, 8748–8754 (2020).
28. Harrington, D. A. & Conway, B. E. Kinetic theory of the open-circuit potential decay method for evaluation of behaviour of adsorbed intermediates: analysis for the case of the H_2 evolution reaction. *J. Electroanal. Chem. Interfacial Electrochem.* **221**, 1–21 (1987).
29. Conway, B. E. & Jerkiewicz, G. Relation of energies and coverages of underpotential and overpotential deposited H at Pt and other metals to the 'volcano curve' for cathodic H_2 evolution kinetics. *Electrochim. Acta* **45**, 4075–4083 (2000).
30. Conway, B. E. & Bai, L. State of adsorption and coverage by overpotential-deposited H in the H_2 evolution reaction at Au and Pt. *Electrochim. Acta* **31**, 1013–1024 (1986).
31. Maoka, T. & Enyo, M. Overpotential decay transients and the reaction mechanism on the Pd-H_2 electrode. *Surf. Technol.* **8**, 441–450 (1979).
32. Devanathan, M. A. V., Stachurski, Z. & Tompkins, F. C. The adsorption and diffusion of electrolytic hydrogen in palladium. *Proc. R. Soc. Lond. A Math. Phys. Sci.* **270**, 90–102 (1962).
33. Ward, T. L. & Dao, T. Model of hydrogen permeation behavior in palladium membranes. *J. Membr. Sci.* **153**, 211–231 (1999).
34. Yun, S. & Ted Oyama, S. Correlations in palladium membranes for hydrogen separation: a review. *J. Membr. Sci.* **375**, 28–45 (2011).
35. Rahimpour, M. R., Samimi, F., Babapoor, A., Tohidian, T. & Mohebi, S. Palladium membranes applications in reaction systems for hydrogen separation and purification: a review. *Chem. Eng. Process. Process Intensif.* **121**, 24–49 (2017).

36. Delima, R. S., Sherbo, R. S., Dvorak, D. J., Kurimoto, A. & Berlinguette, C. P. Supported palladium membrane reactor architecture for electrocatalytic hydrogenation. *J. Mater. Chem. A* **7**, 26586–26595 (2019).
37. Jansonius, R. P. et al. Hydrogenation without H_2 using a palladium membrane flow cell. *Cell Rep. Phys. Sci.* **1**, 100105 (2020).
38. Kurimoto, A., Sherbo, R. S., Cao, Y., Loo, N. W. X. & Berlinguette, C. P. Electrolytic deuteration of unsaturated bonds without using D_2. *Nat. Catal.* **3**, 719–726 (2020).
39. Kurimoto, A. et al. Physical separation of H_2 activation from hydrogenation chemistry reveals the specific role of secondary metal catalysts. *Angew. Chem. Int. Ed.* **60**, 11937–11942 (2021).
40. Delima, R. S. et al. Selective hydrogenation of furfural using a membrane reactor. *Energy Environ. Sci.* **15**, 215–224 (2022).
41. Sherbo, R. S., Kurimoto, A., Brown, C. M. & Berlinguette, C. P. Efficient electrocatalytic hydrogenation with a palladium membrane reactor. *J. Am. Chem. Soc.* **141**, 7815–7821 (2019).
42. Sherbo, R. S., Delima, R. S., Chiykowski, V. A., MacLeod, B. P. & Berlinguette, C. P. Complete electron economy by pairing electrolysis with hydrogenation. *Nat. Catal.* **1**, 501–507 (2018).
43. Yoshitake, H., Kikkawa, T. & Ota, K. Isotopic product distributions of CO_2 electrochemical reduction on a D flowing-out Pd surface in protonic solution and reactivities of 'subsurface' hydrogen. *J. Electroanal. Chem.* **390**, 91–97 (1995).
44. Rock, P. A. Electrochemical double cells. *J. Chem. Educ.* **52**, 787 (1975).
45. Flanagan, T. B. & Oates, W. A. The palladium-hydrogen system. *Annu. Rev. Mater. Sci.* **21**, 269–304 (1991).
46. Tsirlina, G. A., Levi, M. D., Petrii, O. A. & Aurbach, D. Comparison of equilibrium electrochemical behavior of PdHx and $LixMn_2O_4$ intercalation electrodes in terms of sorption isotherms. *Electrochim. Acta* **46**, 4141–4149 (2001).
47. Liu, S., Mu, X., Duan, H., Chen, C. & Zhang, H. Pd nanoparticle assemblies as efficient catalysts for the hydrogen evolution and oxygen reduction reactions. *Eur. J. Inorg. Chem.* **2017**, 535–539 (2017).
48. Thrush, K. A. & White, J. M. Carbon monoxide and hydrogen coadsorption on polycrystalline platinum. *Appl. Surf. Sci.* **24**, 108–120 (1985).
49. Roman, T., Nakanishi, H. & Kasai, H. Coadsorbed H and CO interaction on platinum. *Phys. Chem. Chem. Phys.* **10**, 6052–6057 (2008).
50. Couble, J. & Bianchi, D. Experimental microkinetic approach of the CO/H_2 reaction on Pt/Al_2O_3 using the Temkin formalism. 1. Competitive chemisorption between adsorbed CO and hydrogen species in the absence of reaction. *J. Catal.* **352**, 672–685 (2017).
51. Palazov, A., Kadinov, G., Bonev, C. H. & Shopov, D. Infrared spectroscopic study of the interaction between carbon monoxide and hydrogen on supported palladium. *J. Catal.* **74**, 44–54 (1982).
52. Yu, W.-Y., Mullen, G. M. & Mullins, C. B. Interactions of hydrogen and carbon monoxide on Pd–Au bimetallic surfaces. *J. Phys. Chem. C* **118**, 2129–2137 (2014).

Acknowledgements

We acknowledge C. Costentin, M. Koper and J. Mayer for discussions. The authors thank the entire Surendranath Lab for their support and scientific discussions, with particular acknowledgement towards H. Dinh, A. Chu, W. Howland, T. Marshall-Roth and H. Wang for their helpful discussions and mentorship. The authors would also like to thank C. Kaminsky and J. Ryu for their insights and mentorship. This research was supported by the National Science Foundation, under award number CHE-2102669.

Author contributions

B.Y.T., R.P.B. and Y.S. conceived the research and developed experiments. B.Y.T. conducted the majority of the experiments. R.P.B., K.M.L. and W.L.T. contributed to data collection. B.Y.T. and Y.S. wrote the manuscript with input from all authors.

Competing interests

The authors declare no competing interests.

Additional information

Supplementary information The online version contains supplementary material available at https://doi.org/10.1038/s41929-023-00943-2.

Correspondence and requests for materials should be addressed to Yogesh Surendranath.

Peer review information *Nature Catalysis* thanks Curtis Berlinguette and the other, anonymous, reviewer(s) for their contribution to the peer review of this work.